Reconciling geologic and geodetic fault-slip-rate discrepancies in southern California: consideration of non-steady mantle flow and lower crustal fault creep

Supplementary Online Materials

INTERSEISMIC MODEL: STRESS-DRIVEN CREEP

As stated in the main text, the model used in this study is described in Huang et al. (2010) and Johnson and Fukuda (2010). These studies build on Johnson and Segall (2004) who developed a boundary element solution for stress-driven intersesismic creep below the locking depth of an infinitely-long, strike-slip fault in an elastic plate over a viscoelastic substrate. Above the fault locking depth, periodic earthquakes are imposed and the fault is completely locked between earthquakes. Below the locking depth, the fault creeps as a thin linear viscous shear zone. In this study, and in Huang et al. (2010) and Johnson and Fukuda (2010), we consider the special case of the Johnson and Segall (2004) model in which the viscosity of the shear zone is zero. However, this study is different from Huang et al. (2010) and Johnson and Fukuda (2010) in that we approximate the deep creep on faults with a uniform creep rate proportional to the depth-averaged shear stress rate on the fault (as opposed to considering depth-variable creep rates).

Figure DR1a shows the creep rate below a fault locked down to 10 km depth in an elastic plate of thickness 20 km for different ratios of recurrence time to asthenosphere relaxation time, T/t_R. For the case $T/t_R = 1$, the fault creeps at a nearly steady rate throughout the earthquake cycle and the creep rate tapers from the full long-term fault slip rate at the base of the elastic plate to zero just below the locking depth. As the ratio T/t_R increases, the creep rates vary more significantly throughout an earthquake cycle; early in the cycle the creep rate on the fault might exceed the long-term rate and late in the cycle the creep rate may be less than half the long-term rate. Figure DR1 shows the predicted surface velocities across the fault at different times in the earthquake cycle, expressed as the ratio t/T. Blue curves show the Johnson and Segall (2004) model prediction and the green curves show the Savage and Prescott (1978) model prediction assuming steady creep at the long-term rate below the locking depth. The Savage and Prescott (1978) steady creep model predicts higher velocities than the Johnson and Segall

(2004) model mid-way and late in the earthquake cycle because the creep rate is lower at these times in the Johnson and Segall (2004) model. Figure DR1 suggests that neglecting time-variable fault creep could lead to biased estimates of fault slip rates and locking depths.

The creep rate on the fault is a function of the stress on the fault at any given time which is dependent on the history of slip on the fault. Let T be the recurrence time of earthquakes, let $\dot{s}$ be the long-term fault slip rate, and let $\dot{s}_c(t, z)$ be the instantaneous creep rate at depth z on the fault. We require that the total stress is zero on the creeping part of the fault at some time, t, after initiation of sliding at $t = -\infty$,

$$g_e^U(t - t_{eq}, z, T)\dot{s} + \int_{-\infty}^{t}\int_{H}^{D} g_c^L(t - \tau, \xi, z)\frac{\partial \dot{s}_c(\tau, \xi)}{\partial \xi} d\xi d\tau = 0$$

where the first term gives the stress at depth z and time t due to slip below the locking depth at depth z_0 and time t_0. In this notation, the subscripts on g denote either creep (c) or earthquake slip (e) and the superscript denotes slip on either the upper (U) or lower (L) part of the fault (above or below the locking depth). Johnson and Segall (2004) solved this equation with a boundary element approach. That method is computationally expensive and requires computing the slip at all times and depths throughout all earthquake cycles on all faults. Here we use an approximate form of the equation that can be solved efficiently. The approach is to assume a simple slip history, illustrated in Figure DR2, in which the fault slips during earthquakes uniformly from the surface to the locking depth by amount $\dot{s}T$ and uniformly from the locking depth to the bottom of the elastic plate by a lesser amount, $(\dot{s} - \dot{s}_c)T$, where $\dot{s}_c$ is the yet-to-be-determined steady interseismic creep rate. This slip rate history is computed assuming the instantaneous stress rate on the fault at the time of observation is zero

$$\dot{g}_e^U(z, t - t_e q)\dot{s}T + \dot{g}_e^L(z, t - t_e q)(\dot{s} - \dot{s}_c)T + \dot{g}_c^L(z)\dot{s}_c = 0$$

where the dot denotes time derivative, $\dot{g}_e^U$ is the same as above, $\dot{g}_e^L(z, t - t_{eq})$ is the stressing rate at depth z and time $t - t_{eq}$ due to coseismic slip below the locking depth, and $\dot{g}_c^L(z)$ is the stressing rate at depth z due to steady creep below the locking depth.

The interseismc creep rate is then,

$$\dot{s}_c = \dot{s}\frac{T\left(\dot{g}_e^U + \dot{g}_e^L\right)}{\dot{g}_c^L - T\dot{g}_e^L}$$

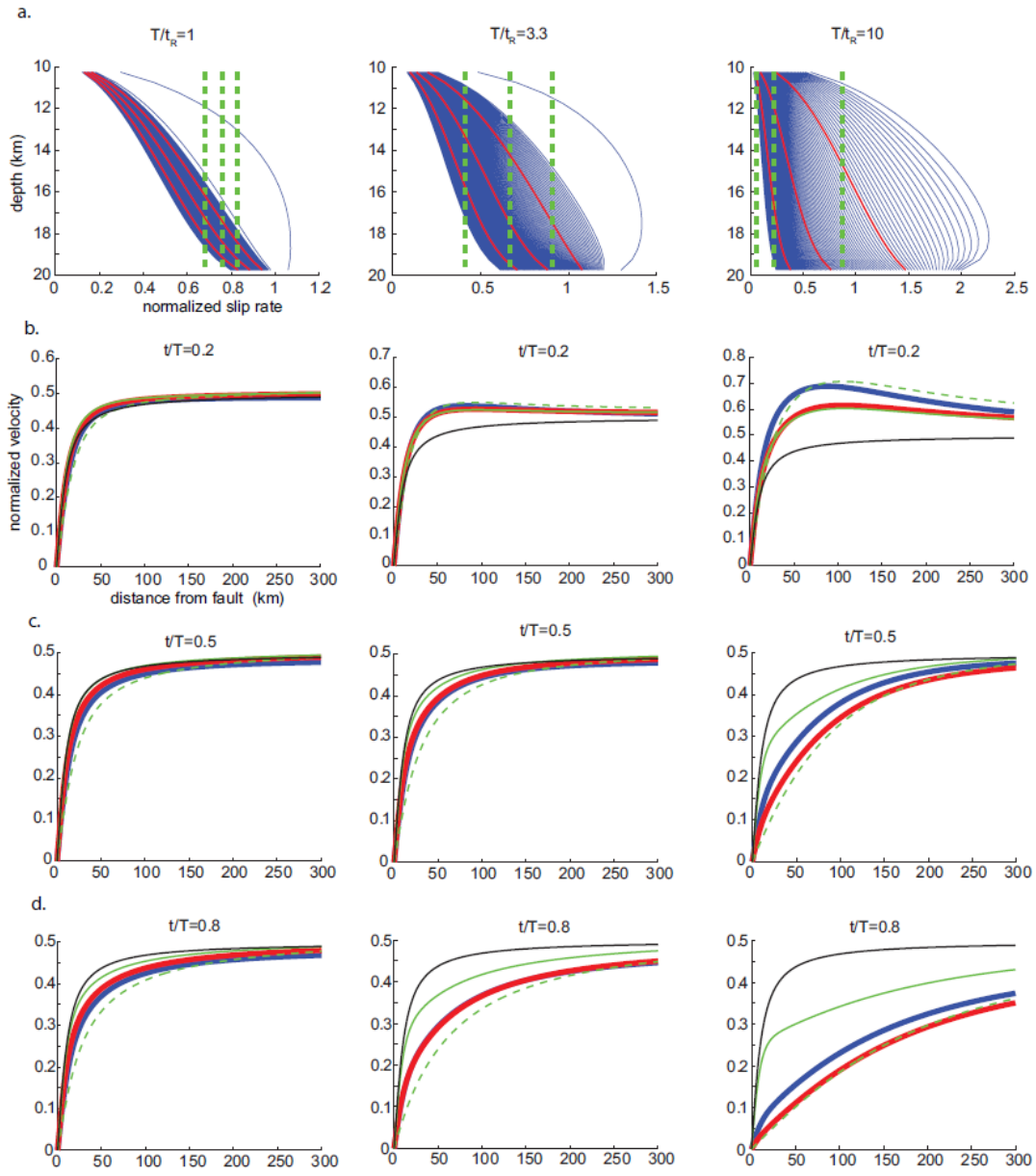

Figure DR1. (a) Interseismic creep rates predicted by the Johnson and Segall (2004) model. Each blue curve is the creep rate at equally spaced times in an earthquake cycle for various cycle parameters, T/t_R. The vertical dashed green lines are the approximate constant-stress model predictions of instantaneous creep rate at the observation time and the red curves are the corresponding instantaneous creep rates in the Johnson and Segall (2004) model at the same times. (b)-(d) compare surface velocity profile predictions for

several models (think black – buried elastic screw dislocation, solid green – Savage and Prescott model with deep creep at the long-term slip rate, dashed green – Savage and Prescott model with no deep creep, heavy blue line – Johnson and Segall (2004) model, heavy red line – approximate constant-stress model).

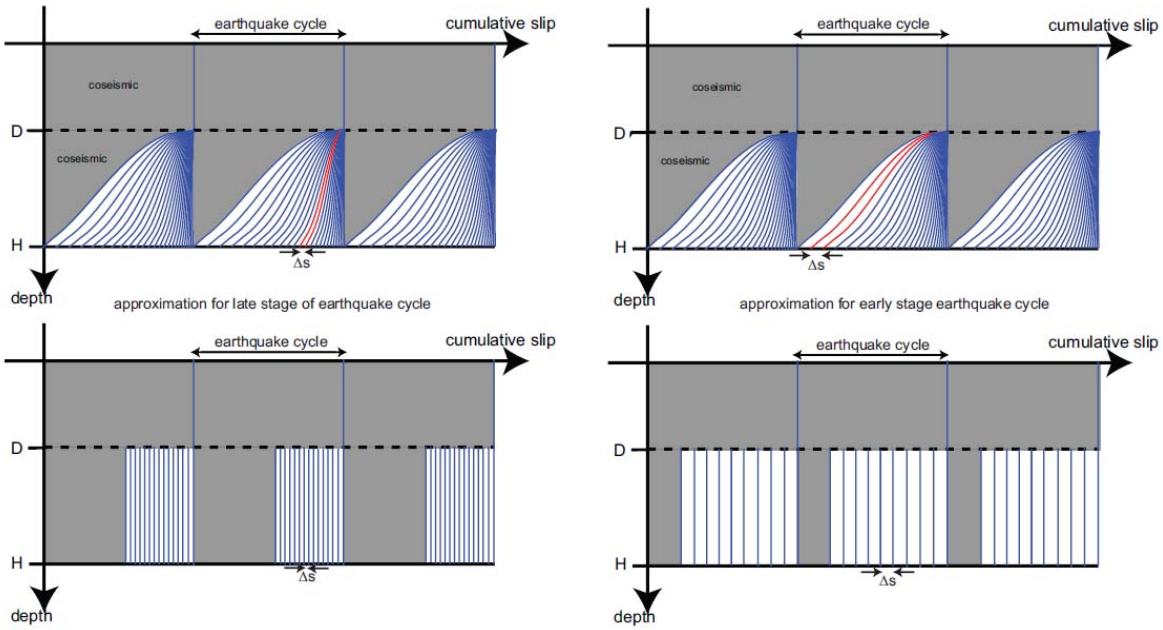

Figure DR2. Top: slip evolution over three earthquake cycles computed using the Johnson and Segall (2004) model. Bottom: assumed slip history in the approximate constant-stress model.

EXPLANATION OF SLIP RATE DATA

We found that along most of major faults, geologic slip rates adopted by WGCEP (2008) are in agreement with other published studies, except for the San Bernardino and Coachella segments of the San Andreas fault and San Jacinto fault. Along the San Bernardino segment, fault-slip rates decrease north to south from 25 mm/yr (Weldon and Sieh, 1985) to 11 mm/yr (McGill et al., 2008). WGCEP (2008) assigns 18 and 20 mm/yr for the San Jacinto fault and the Coachella segment of the San Andreas fault, respectively. However, other paleoseismology data suggest ~12 mm/yr for the central San Jacinto fault (Rockwell et al., 1990, Blisniuk et al., 2010) and ~16 mm/yr for the northern Coachella segment (van der Woerd et al., 2006). Paleoseismology data suggest the slip rate of the southern Coachella segment close to the Salton Sea is 5-8 mm/yr (Shuttle et al., 2002). In our model, we chose 13 mm/yr (Blisniuk et al., 2010) and 16 mm/yr (van der Woerd et al., 2006) for the two faults with large uncertainties (10 mm/yr) to allow possible

variation in the fault slip rates. For the southern Mojave ECSZ, we used the rate of ~8 mm/yr calculated from the sum geologic slip rates of 6.2 ± 1.9 mm/yr plus 10-30% of fault slip absorbed by distributed shear in zones associated with faults (Oskin et al., 2008).

EXPLANATION OF EARTHQUAKE TIMING PARAMETERS

We adopt the data of recurrence intervals from WGCEP (2008) for the San Andreas, San Jacinto, and Garlock faults. We have assigned a shorter recurrence interval for the Garlock fault compared to the preferred recurrence interval of ~1200 years from WGCEP (2008) because the average repeat time is about 675-690 for the most recent events. For other faults, we assign recurrence intervals based on the information from the southern California fault map of the SCEC data center.

We also take data of time since last earthquake from WGCEP (2008) and other paleoseismology studies. We also assigned shorter time since last earthquake for the San Jacinto fault compared to 200 year repeat time adopted by WGCEP (2008) since some sections of the San Jacinto and Superstition Mountains fault have ruptured at least five times since 1899 (Lundgren et al., 2009).

Even though the surface velocities have been corrected for the coseismic deformation due to the 1992 Landers and 1999 Hector Mine earthquakes, a shear strain rate map derived from the velocity field (Fig. DR3) shows the concentration of strain rates in the southern Mojave ECSZ. The strain rates here derived from the SCEC CMM3 data set are higher than the rates derived from trilateration data prior to 1992 (Sauber et al., 1994), indicating this might be due to post-seismic effects of the Landers and Hector Mine earthquakes. Since we simplified the fault geometry in the ECSZ as one through-going fault, we use different composite time since last earthquakes for this model fault to examine the range of model slip rates corresponding to the timing since last earthquakes. If we assume that the composite time since the last earthquake is 100 years, the model slip rate is ~7 mm/yr. If we assume the composite time since last earthquake is 300-500 years, the model rate is ~15-20 mm/yr. Therefore, our estimates of slip rates across the southern ECSZ are highly sensitive to the assumed timing of past earthquakes.

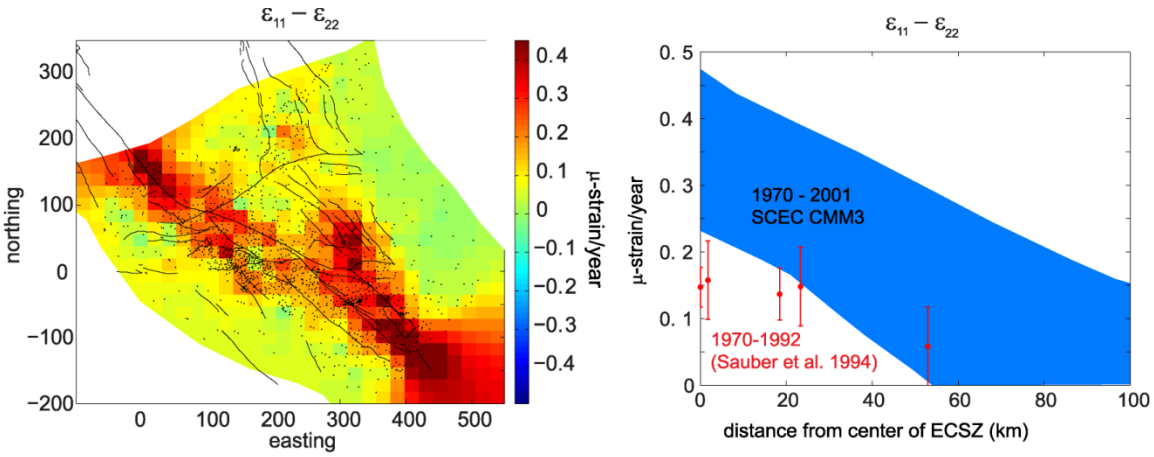

Figure DR3. (Left) Shear strain rate map derived from SCEC CMM 3. (Right) Comparison of shear strain rates derived from SCEC CMM3 (1970-2001) and rates from trilateration data (1970-1992) in the southern ECSZ.

MODEL RESULTS AND VISCOELASTIC EFFECTS

Table DR1 shows the summary of our model slip rates for the major faults and the comparison of geologic rates and model rates from elastic block models. We can reconcile geologic and geodetic fault slip rates by using our viscoelastic model. In order to estimate the viscosity structure in southern California, we conducted a grid search to find an optimal viscosity for the lower crust/upper mantle with an assumption of a viscosity of 6×10^{18} Pa s for the mantle substrate. Our grid search result shows that the optimal viscosity for the lower crust/upper mantle is 2×10^{20} Pa s (Fig. DR4).

Our viscoelastic model is able to reconcile fault slip rates, especially along the Mojave segment of the San Andreas fault, San Jacinto fault, Garlock fault, and ECSZ. In other words, our viscoelastic model estimates higher slip rates on the Garlock fault and the Mojave segment of the San Andreas fault and lower slip rates across the ECSZ than elastic models. This is because our model predicts fast (slow) deformation rates in the early (late) stage of earthquake cycles due to the postseismic relaxation of viscous flow in the mantle. Figure DR5 shows the predicted surface velocity profile perpendicular to the Mojave segment of the San Andreas fault at different times. The predicted velocities for different times since the last earthquake shows that most of the rapid postseismic relaxation occurs in about 10 years following earthquakes and there is only a few mm/yr of variation in velocities after the first 10 years. There is an indication that earthquakes in the southern ECSZ occur in clusters that repeat about every 5000 years with the recent 1992 Landers and 1999 Hector Mine earthquakes being part of the most recent cluster

(Rockwell et al., 2000; Dolan et al., 2007). Therefore, we have adopted a composite recurrence time of 5000 years for the southern ECSZ and assumed that we are currently observing deformation in the early phase of this cycle ($t_{eq}/T = 0.02$). The San Jacinto fault and ECSZ are discontinuous. For the convenience of block model construction and calculations, we simplify the geometry and rupture length to achieve an overall, first-order deformation for these two areas. Thus, we assign one recurrence interval and time since last earthquake for each of them. The true rupture patterns of individual segments could be more complicated.

Table DR1. Summary of geologic and geodetic fault-slip rates along major fault in southern California.

Fault segment	Geologic rates (mm/yr)		Bennet et al. (1996)	Becker et al. (2004)		Meade and Hager (2005)	McCaffrey (2005)	This study
				only GPS	Joint inversion			
SAF-Carrizo	33.9 ± 2.9	Sieh and Jahns, 1984	N/A	33.1 ± 9	26.8 ± 8	35.9 ± 0.7	30.4 ± 0.1	33.1 ± 1.3
SAF-Mojave	30 ± 10	Matmon et al., 2005; Weldon et al., 2004	33±2	9.4 ± 13	15.7 ± 12	14.3 ± 1.2	25.1 ± 0.3	26.0 ± 1.5
SAF-San Bernardino	10 ± 5.5	McGill et al., 2008	22±2	−2.3 ± 15	0.9 ± 12	5.1 ± 1.5	19.1 ± 4.8	8.2 ± 1.9
SAF-Coachella	15.9 ± 3.4	van der Woerd et al., 2006	26±2	23.0 ± 8	22.9 ± 8	23.3 ± 0.5	25.6 ± 0.3	17.2 ± 1.1
San Jacinto	10 - 14 [a]	Blisniuk et al., 2010	9±2	15.3 ± 11	14.5 ± 9	11.9 ± 1.2	12.3 ± 1.2	10.8 ± 0.8
Elsinore	5.1 ± 2.1	Millman and Rockwell, 1986	6±2	3.7 ± 7	3.7 ± 6	2.7 ± 0.6	1.3 ± 0.1	3.3 ± 0.9
Garlock			N/A	−4.8 ± 14	−3.1 ± 10			
West	−8 ± 2.7	McGill et al., 2009				−3.2 ± 1.5	−4.9 ± 0.2	−9.5 ± 1.8
Central	−6.8 ± 1.3	Carter, 1994				−1.8 ± 1.5	−9.3 ± 6	−8.9 ± 1.8
East	~ −2.5	McGill, 1998				−1.1 ± 1.9	−1.8 ± 0.2	−6.2 ± 2.3
ECSZ	7.9 ± 2.6 [b]	Oskin et al., 2008	N/A	18.1 ± 19 [c]	13.9 ± 17	15 ± 3.6 [d]	9.8 ± 0.3	7.2 ± 0.3
Imperial	15 - 20	Thomas and Rockwell, 1996	35±2	39.5 ± 7	38.5 ± 5	36.1 ± 0.7	21.9 ± 0.8	36.6 ± 1.0
Santa Cruz Island	−1 ± 0.5 [e]	WGCEP, 2008	N/A	−2.5 ± 11	−2.4 ± 11	N/A	−3.4 ± 0.2	0.4 ± 0.1
Death Valley	5 ± 3 [e]	WGCEP, 2008	N/A	4.6 ± 8	4.1 ± 8	2.4 ± 1.2	2.5 ± 0.1	5.0 ± 1.4
Panamint Valley	2.5 ± 1 [e]	WGCEP, 2008	N/A	N/A	N/A	3.1 ± 1.3	2.0 ± 0	2.0 ± 1.2
Sierra Nevada - Little Lake	0.7 ± 0.4 [e]	WGCEP, 2008	N/A	1.0 ± 10	6.8 ± 8	3.5 ± 0.9	5.6 ± 0.4	5.0 ± 0.4
Hosgri	2.5 ± 1	Hanson and Lettis, 1994	N/A	N/A	N/A	3.9 ± 0.6	3.4 ± 0.8	6.0 ± 1.0
Newport - Inglewood	1 ± 0.5 [e]	WGCEP, 2008	3 ± 3	N/A	N/A	0.8 ± 1.6	3.1 ± 0.1	2.3 ± 0.5
Palos Verdes	3 ± 1 [e]	WGCEP, 2008	N/A	N/A	N/A	3.4 ± 1.4	4.3 ± 0.9	4.5 ± 1.0
Santa Cruz - Sabta Catalina Ridge	N/A		4 ± 3	N/A	N/A	N/A	N/A	4.0 ± 1.8
San Gabriel	1 ± 0.5 [e]	WGCEP, 2008	N/A	N/A	N/A	3.8 ± 2.2	2.1 ± 1.3	0.3 ± 0.5

[a]: Blisniuk et al. (2010) summarize their results and many previous rates to have this estimate.
[b]: This rate is the sum of fault-slip rates and distributed shear across six faults
[c]: The rate is the sum of model rates of ECSZ east and ECSZ west segments
[d]: The rate is the sum of model rates of Blackwater-Landers, Helendale, Goldstone, and eastern Mojave segments.

[e]: Expert opinion slip rates from WGCEP (2008)

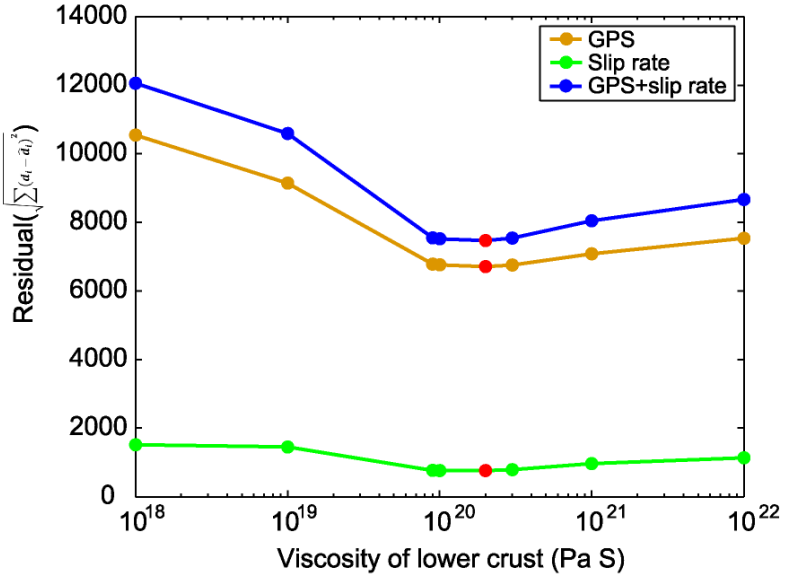

Figure DR4. Plot the model residuals versus the viscosities of the lower crust. Browns are the GPS residuals, greens are the slip-rate residuals, and blues are the sum of GPS and geologic rate The minimum residual occurs at the viscosity of 2×10^{20} Pa S.

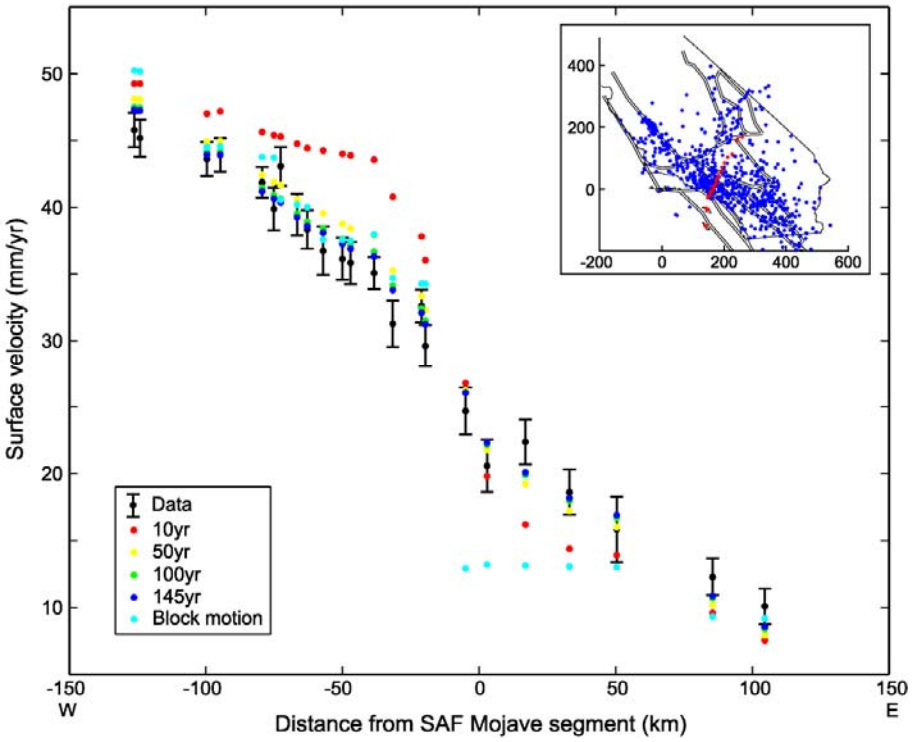

Figure DR5. Surface velocity transect across the Mojave segment of the San Andreas fault. Black bars are data from SCEC CMM 3. Red, yellow, green, and blue dots represent surface velocities with time since last earthquake of 10, 50, 100, and 145 years, respectively, for the Mojave segment. Cyan dots are block-motion rates.

REFERENCES CITED

Blisniuk, K., Rockwell, T., Owen, L.A., Oskin, M., Lippincott, C., Caffee, M.W., and Dortch, J., 2010, Late Quaternary slip rate gradient defined using high-resolution topography and ^{10}Be dating of offset landforms on the southern San Jacinto Fault zone, California: Journal of Geophysical Research, 115, B08401, doi: 10.1029/2009JB006346.

Carter, B., 1994, Neogene offsets and displacement rates, central Garlock fault, California, *in* McGill, S.F., and Ross, T.M., eds., Geological investigations of an active margin: Redlands, California, San Bernardino County Museum Association, p. 348–356.

Hanson, K., and Lettis, W.R., 1994, Estimated Pleistocene slip-rate for the San Simeon fault zone, south-central coastal California, *in* Alterman, I.B., McMullen, R.B., Cluff, L.S., and Slemmons, D.B., eds., Seismotectonics of the Central California Coast Ranges: Geological Society of America Special Paper 292, p. 133-150.

Johnson, K.M. and Segall, P., 2004, Viscoelastic earthquake cycle models with deep stress-driven creep along the San Andreas fault system: Journal of Geophysical Research, v. 109, B10403, doi: 10.1029/2004JB003096.

Li, V., and Rice, J., 1987, Crustal deformation in great California earthquake cycles: Journal of Geophysical Research, 92, 11,533-11,551.

Lundgren, P., Hetland, E.A., Liu Z., and Fielding, E.J., 2009, Southern San Andreas-San Jacinto fault system slip rates estimated from earthquake cycle models constrained by GPS and interferometric synthetic aperture radar observations: Journal of Geophysical Research, v. 114, B02403, doi:10.1029/2008JB005996.

Matmon, A., Schwartz, D.P., Finkel, R., Clemmens, S., and Hanks, T., 2005, Dating offset fans along the Mojave section of the San Andreas fault using cosmogenic ^{26}Al and ^{10}Be: GSA Bulletin, v. 117, p. 795-807, doi: 10.1130/B25590.1.

McCaffrey, R., 2005, Block kinematics of the Pacific-North America plate boundary in the southwestern United Sates from inversion of GPS, seismological, and geologic data.: Journal of Geophysical Research, v. 110, B07401, doi: 10.1029/2004JB003307.

McGill, S.F., 1998, Preliminary slip-rate estimate for the Owl Lake fault, California, *in* Calzia, J.P., and Reynolds, R.E., eds., Finding faults in the Mojave: San Bernardino County Museum Association Quarterly, v. 45, nos. 1 and 2, p. 84–87.

McGill, S.F., Weldon, R.J., and Owen, L., 2008, Preliminary slip rates along the San Bernardino strand of the San Andreas fault: southern California Earthquake Center Annual Meeting, Proceedings and Abstracts, v. 18.

McGill, S.F., Wells, S.G., Fortner, S.K., Kuzma, H.A., and McGill, J.D., 2009, Slip rate of the western Garlock fault, at Clark Wash, near Lone Tree Canyon, Mojave Desert, California: GSA Bulletin, v. 121, p. 536-554, doi: 10.1130/B26123.1; 14.

Meade, B.J., and Hager, B.H., 2005, Block models of present crustal motion in southern California constrained by GPS measurements: Journal of Geophysical Research, v. 110, B03403, doi: 10.1029/2004JB003208.

Millman, D.E., and Rockwell, T.K., 1986, Neotectonics of the Elsinore fault in Temescal Valley, California: Geological Society of America Guidebook and Volume, 82nd Annual Meeting, v. 82, p. 159-166.

Oskin, M., Perg, L., Shelef, E., Strane, M., Gurney, E., Singer, B., and Zhang, X., 2008, Elevated shear zone loading rate during an earthquake cluster in eastern California: Geology, v. 36, p. 507-510.

Rockwell, T.K., Loughman, C., and Merifield, P., 1990, Late Quaternary rate of slip along the San Jacinto fault zone near Anza, southern California: Journal of Geophysical Research, v. 95, p. 8593-8605.

Sauber, J., Thatcher, W., Solomon, S.C., and Lisowski, M., 1994, Geodetic slip rate for the eastern California shear zone and the recurrence time of Mojave desert earthquakes: Nature, 367, 264-266.

Savage, J.C., and Prescott, W.H., 1978, Asthenosphere readjustment and the earthquake cycle: Journal of Geophysical Research, v. 83, p. 3369-3376.

Sieh, K.E., and Jahns, R.H., 1984, Holocene activity of the San Andreas fault at Wallace creek, California: Geological Society of America Bulletin, v. 95, p. 883-896.

Thomas, A.P., and Rockwell, T.K., 1996, A 300- to 550- year history of slip on the Imperial fault near the U.S.-Mexico border: Missing slip at the Imperial fault bottleneck: Journal of Geophysical Research, 101, 5987-5997.

van der Woerd, J., Klinger, Y., Sieh, K., Tapponnier, P., Ryerson, F.J., and Mériaux, A.-S., 2006, Long-term slip rate of the southern San Andreas fault from ^{10}Be-^{26}Al surface exposure dating of an offset alluvial fan. Journal of Geophysical Research: v. 111, B04407, doi:10.1029/2004JB003559.

Weldon, R.J., and Sieh, K., 1985, Holocene rate of slip and tentative recurrence interval for large earthquakes on the San Andreas fault, Cajon Pass, southern California: Geological Society of America Bulletin, v. 96, p. 793-812.

Weldon, R., Fumal, T., and Biasi, Glenn, 2004, Wrightwood and the earthquake cycle: What a long recurrence record tells up about how fault faults work: GSA Today, v. 14, doi: 10.1130/1052-5173.

Working Group on California Earthquake Probabilities, 2008, The uniform California earthquake rupture Forecast, version 2 (UCERE 2): USGS Open File Report 2007-1437, 104p.